JOURNAL OF THERMOPHYSICS AND HEAT TRANSFER
Vol. 16, No. 2, April–June 2002

Electrohydrodynamically Augmented Micro Heat Pipes

Zhiquan Yu,* Kevin Hallinani,† Wilbur Bhagat,* and Reza Kashani‡
University of Dayton, Dayton, Ohio 45469-0210

An experimental investigation was conducted to evaluate the potential benefits of electrohydrodynamic (EHD) forces on the operation of micro heat pipes. In these experiments, electric fields were used to orient and guide the flow of the dielectric liquid within the micro heat pipe from the condenser to the evaporator. The experiments indicate the heat transport capability of the EHD micro heat pipes is increased by up to six times of that of conventional ones. In parallel, an analytical model was developed to predict the maximum heat transport capability for various electric field intensities and micro heat pipe geometries. The analytical model agrees well with the experimental results for the geometry studied experimentally. The model shows that large pore sizes are optimal from a heat transport capacity perspective. Finally, a critical assessment of the experimental results suggest an alternative design capable of achieving as much as a 180 times improvement in the heat transport capacity in comparison to traditional micro heat pipes.

Nomenclature

A	=	cross-sectional area, m^2
a	=	channel depth, m
C	=	coefficient
d	=	width of pipe plus space between pipes, m
E	=	electric field intensity, V/m
f	=	friction factor
g	=	gravitational acceleration, m/s^2
h	=	spacing of the electrodes, m
L	=	length, m
L_{eff}	=	effective length, m
M	=	parameter defined in Eq. (10)
P	=	pressure, N/m^2
Q	=	total heat input into device, W
q	=	heat transport for one channel, W
q''	=	heat flux, W/m^2
Re	=	Reynolds number
R_h	=	hydraulic radius, m
r	=	meniscus radius of curvature, m
T	=	temperature, K
U	=	velocity of fluid moving, m/s
V	=	applied voltage, V
w	=	channel width, m
ε	=	permittivity, $\varepsilon_0\kappa$
κ	=	dielectric constant
λ	=	latent heat of vaporization, J/kg
μ	=	viscosity, Ns/m^2
ρ	=	density, kg/m^3
σ	=	surface tension, N/m
ψ	=	tilt angle

Subscripts

c	=	capillary
EHD	=	electrohydrodynamic
e	=	evaporator
h	=	hydraulic
l	=	liquid
max	=	maximum
v	=	vapor

Received 3 April 2000; revision received 15 October 2001; accepted for publication 23 October 2001.

*Graduate Research Assistant, Department of Mechanical and Aerospace Engineering.

†Professor, Chairman of the Department of Mechanical and Aerospace Engineering; khallina@engr.udayton.edu.

‡Associate Professor, Department of Mechanical and Aerospace Engineering.

Introduction

MICRO heat pipe devices have drawn much attention for their promise to dissipate high-power densities since Cotter[1] first proposed them. Their promise comes from the effective heat transport associated with phase change and their small geometry. In general, a micro heat pipe consists of a small noncircular channel that utilizes sharp angled corner regions as liquid arteries (wick structure) to provide liquid flow from the condenser to the evaporator region. The heat applied to the evaporator end vaporizes the working liquid in that region, forcing it to the cooler end, where it condenses and gives up the latent heat of vaporization. A typical micro heat pipe has a hydraulic diameter ranging from 10 μm to several millimeters and a length of up to several centimeters. By definition, a micro heat pipe requires the Bond number ($Bo = \rho g R_h^2/\sigma$) to be on the order 1 or less. Many studies have been conducted on different kinds of micro heat pipe.[2–7] To date the maximum heat flux dissipated with these devices has been 60 W/cm^2 (Ref. 8).

One of the factors that limits the heat transport capacity of micro heat pipes is the large viscous losses associated with the transport of the liquid from the condenser to the evaporator.[9,10] As the heat input is increased, these losses increase. At large heat inputs, the liquid flow rate cannot sustain the evaporation. When this occurs, the evaporator region is said to dry out. This limitation is called capillary limitation. Another shortcoming is that conventional micro heat pipes are passive in nature and do not allow for active control of the system temperature. Thus, as the heat input increases, so does the temperature of the heat source.

The present research is premised on the assumption that both augmentation of the heat transport capacity and active thermal control of micro heat pipes can be achieved through the application of a static electric field. When an electric field is strategically applied within micro heat pipes at the liquid–vapor interfaces that are internally present, dielectrophoretic electrohydrodynamic forces can be induced due to the discontinuity of the electrical permittivity of the medium. These forces can contribute to a pressure jump condition at the interface, effectively reducing the liquid pressure in the region affected by the field. This pressure reduction can be used to augment the flow of liquid from the condenser to the evaporator region.

Jones[11] first proposed replacing the capillary wick structure in a heat pipe with electrodes. The concept was demonstrated successfully by Jones and Perry[12] and Jones.[13] Their results showed that

the electric field was able to communicate working fluid between the condenser and the evaporator enabling the functioning of the heat pipes, but the performance was poor in comparison to the existing capillary-driven heat pipes. Loehrke and Debs[14] improved the electrohydrodynamic (EHD) heat pipe of Jones and Perry and were able to achieve equivalent thermal performance of conventional axial-groove heat pipes. More recently, Bryan and Seyed-Yagoobi[15] performed an experimental study on a monogroove EHD heat pipe. About 100% enhancement in the heat transport capacity was achieved in their experiments as a result of the EHD pumping.

Hallinan et al.[16] conducted experimental studies on electrohydrodynamic micro heat pipe arrays. Their experiments were conducted on a micro heat pipe array having multiple parallel 1 mm (wide) × 0.6 mm (deep) grooves. The results of their experiments showed that for low heat input the electric field had little effect on heat transport because capillary pressure was sufficient to sustain liquid to the evaporator. However, at heat inputs sufficient to cause evaporator dry out, the application of an electric field had the effect of reducing the heat source temperature.

Based on the promising initial work of Hallinan et al.,[16] more detailed experiments are conducted to further demonstrate the promise of using electrostatic fields to augment the heat transport capacity of EHD-assisted micro heat pipes. Additionally, to better generalize the results for various fluids and micro heat pipe geometry, an analytical model of an EHD-assisted micro heat pipe is developed, which can be used to predict the maximum heat transport capacity and the optimum geometry.

EHD-Assisted Micro Heat Pipe Concept

The EHD micro heat pipe was designed to rely on a dielectrophoretic force to augment the liquid flow from the condenser to the evaporator.[13] This force results from application of an electric field at a liquid–vapor interface. The physical explanation of the force derives from that the polarizing effect of the electric field is greater in the liquid phase, due to the larger electrical permittivity. When an electric field is applied, the molecules of the dielectric fluid present within the micro heat pipe are polarized and dipoles form. In the electric field, the dipoles and other polarized molecules tend to become statistically more ordered and, therefore, exhibit a minimum-energy state. Therefore, the liquid tends to fill the regions of higher electric field intensity due to the requirement of minimizing energy. Jones[13] described that, in EHD heat pipe, polarization force collected the dielectric liquid in regions of higher electric field intensity. Based on thermodynamics theory, Melcher[17] discussed the phenomena that dielectric liquid tended to fill the region where the electric field is strongest. He performed his model analysis using Bernoulli's equation, relating potential energy to the polarization force.

Based on this reasoning, the experimental model shown in Fig. 1a was designed. In this design, the electrodes were located in the evaporator, where the working liquid is needed. These electrodes were placed only over every other groove to draw liquid to the evaporator along these grooves while permitting a vapor return path to the condenser along adjacent grooves. In this configuration, Fig. 1b shows the ideal liquid orientation within the micro heat pipe when the electric field applied, with liquid filling the grooves where the electrodes are present and receding in the grooves without electrodes. For the electrode configuration employed, the localized electric field in the evaporator draws liquid into the evaporator. As such, the heat transport capacity of the micro heat pipe can be increased.

Modeling of EHD Heat Micro Pipes

The model developed here follows that of Ma and Peterson[6] for a conventional micro heat pipe, differing primarily in the inclusion of dielectrophoretic EHD forces. The model is subject to the following assumptions: steady-state flow, constant fluid properties, a nearly horizontal configuration, constant meniscus radius of curvature at a given axial location, constant vapor temperature, and constant surface tension. Also, only axial variations in temperature and meniscus shape are considered.

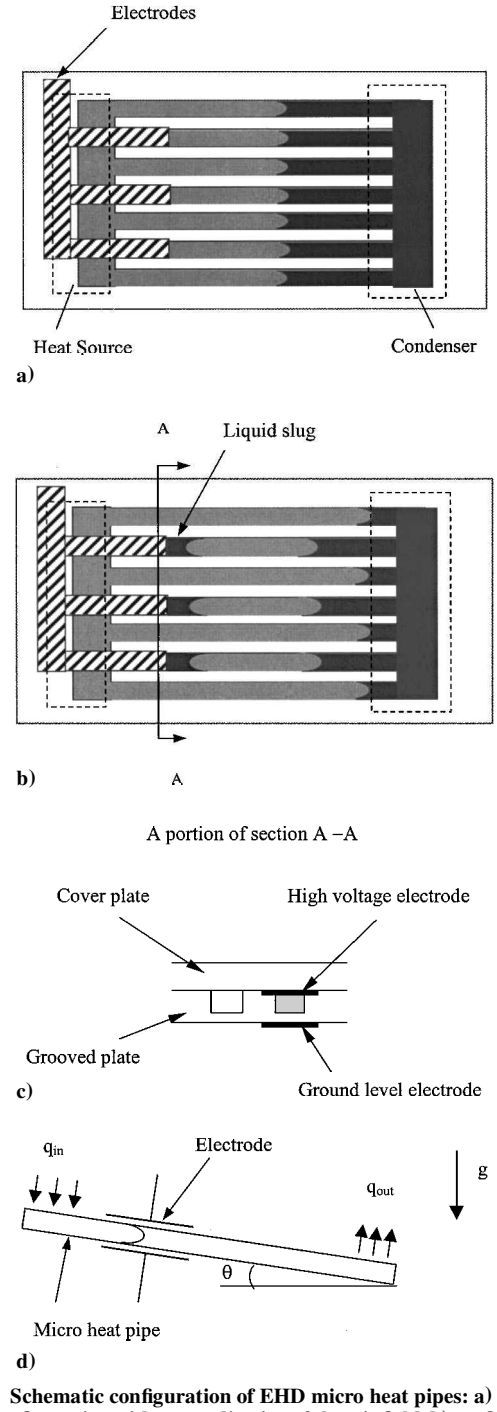

Fig. 1 Schematic configuration of EHD micro heat pipes: a) top view of the configuration without application of electric field, b) configuration with application of electric field, c) schematic of the sandwich electrode structure at A–A section, and d) side view of experimental setup.

At steady state, the operation of EHD micro heat pipes requires that the pressure potential provided by the combination of EHD force and the capillary force be greater than the sum of all the pressure drops occurring throughout the liquid and vapor flow paths. This requirement can be expressed as[9]

$$\Delta P_{\mathrm{EHD}} + \Delta P_c \geq \Delta P_v + \Delta P_l + \Delta P_+ + \Delta P_{\mathrm{slug}} \qquad (1)$$

where ΔP_+ is the normal hydrostatic pressure drop, which can be neglected in the present model because of the assumed horizontal operation, and ΔP_{slug} is the pressure gradient in the liquid slug located beneath the electrodes. Here, the EHD pumping pressure ΔP_{EHD} can be found from Maxwell stress tensor (see Ref. 18, pp. 161–167)

$$T_{ij} = \varepsilon E_i E_j - (\varepsilon/2)(E_k E_k)\delta_{ij} \qquad (2)$$

where δ_{ij} is the Kronecker delta. In the present model, the main electric field direction is defined as y, and so E_x and E_z are much less than E_y. Thus, the stress tensor is given as $T_{yy} = \frac{1}{2} \cdot \varepsilon E^2 = P$. At the interface in the liquid phase, $P_l = \frac{1}{2} \cdot \varepsilon_l E^2$, and in the vapor phase, $P_v = \frac{1}{2}\varepsilon_v E^2$. The electric field is assumed to be uniform in present model. Therefore, the pressure discontinuity at the liquid–vapor interface due to the applied electric field is

$$\Delta P_{\mathrm{EHD}} = \tfrac{1}{2}(\varepsilon_l - \varepsilon_v)E^2 \tag{3}$$

Here ΔP_{EHD} acts normally from liquid to vapor. In present model, ΔP_{EHD} is assumed to be dominated by dielectrophoretic forces. Electrostriction forces owing to the compressibility of the vapor phase are proportional to $E^2\varepsilon_0(\kappa_v - 1)$ (Ref. 19), whereas dielectrophoretic forces are proportional to $E^2\varepsilon_0(\kappa_l - \kappa_v)$. For the working fluid considered (pentane), $\kappa_l = 1.8371$ and $\kappa_v \cong 1$. Therefore, electrostriction forces are very small compared with the dielectrophoretic forces.

Based on the Laplace–Young equation, ΔP_c arises from the capillary pressure differences between the evaporator and condenser ends and can be written as

$$\Delta P_c = \sigma(1/r_{c,e} - 1/r_{c,c}) \tag{4}$$

where $r_{c,e}$ is the minimum meniscus radius of the curvature in the evaporator and $r_{c,c}$ is the average meniscus radius of curvature occurring in the condenser. The minimum meniscus radius in the evaporator is defined as

$$r_{c,e} = 3\sigma/[4 \cdot (\sigma/r_{c,c} + \Delta P_v + \rho_l g L \sin\psi)] \tag{5}$$

Note that the application of electric field influences to some extent the wetting ability of the working liquid; therefore $r_{c,e}$ is affected by the electric field for the present analysis. Hence, the use of Eq. (5) provide an approximate evaluation for $r_{c,e}$. The average meniscus radius in the condenser is set equal to half of the width of channel.

The pressure drops in the micro heat pipe array are shown schematically in Fig. 2, and they are determined as follows. The vapor pressure drop ΔP_v based on momentum conservation is given as

$$\Delta P_v = \frac{f_v \cdot Re_{h,v}\mu_v}{2(r_{h,v})^2 A_v \rho_v \lambda} L_{\mathrm{eff}} q \tag{6}$$

The liquid pressure drop ΔP_l is given as

$$\Delta P_l = \left[\frac{f_l \cdot Re_{h,l}\mu_l L_{\mathrm{eff}}}{2C_1\left(C^* C_2 r_{c,e}\right)^4 \rho_l \lambda}\right] \cdot q \tag{7}$$

where C_1 and C_2 are coefficients depending only on the channel angle of the groove and the contact angle of the liquid. They can be determined using the equations derived by Ma and Peterson.[6] C^* may be determined as

$$C^* = \tfrac{1}{2}(1 + r_{c,c}/r_{c,e}) \tag{8}$$

As seen in Fig. 1b, the working liquid was drawn to the region of electric field forming liquid slugs beneath the electrodes. The pressure losses in this slug ΔP_{slug} can be derived for laminar flow in a square channel filled with liquid:

$$\Delta P_{\mathrm{slug}} = \frac{12\mu_l}{wa^3\rho_l\lambda} L_{\mathrm{slug}} q \tag{9}$$

where L_{slug} is the length of the slug on both side of the trapped vapor bubble.

When all of the preceding expressions are substituted into Eq. (1) and rearranged, a relationship between thermal throughput q and electric field intensity E is found as follows:

$$q = (1/M)\left[(\varepsilon_l - \varepsilon_v)(E^2/2) + \sigma(1/r_{c,e} - 1/r_{c,c})\right] \tag{10}$$

In this equation, M can be considered as a parameter depending on the geometry of the micro heat pipe and the properties of the working fluid, and it is expressed as

$$M = \frac{12\mu_l L_{\mathrm{slug}}}{wa^3\rho_l\lambda} + \frac{f_v Re_{h,v}\mu_v L_{\mathrm{eff}}}{2r_{h,v}^2 A_v \rho_v \lambda} + \frac{f_l Re_{h,l}\mu_l L_{\mathrm{eff}}}{2C_1\left(C^* C_2 r_{c,e}\right)^4 \rho_l \lambda} \tag{11}$$

Once the applied electric field intensity and the minimum meniscus radius of the curvature occurring in the evaporator are given, the maximum heat transport capacity can be predicted by Eq. (10).

The distribution of the electric field is complicated because of the presence of multiphase. Therefore, the electric field used here might be referred to as apparent electric field. The actual electric field in liquid may be determined using Crowley's formula (see Ref. 18, pp. 19–20)

$$E_l = \frac{-(\varepsilon_s/\varepsilon_l)(V/h)}{1 + [(\varepsilon_s/\varepsilon_l) - 1](a/h)} \tag{12}$$

where ε_s is the glass permittivity.

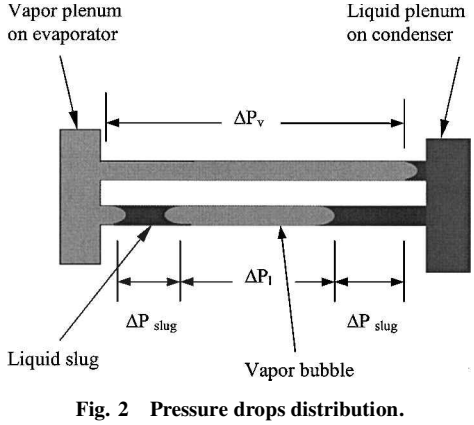

Fig. 2 Pressure drops distribution.

Experiments

The micro heat pipe array used in the present experiments was manufactured from a 1-mm-thick glass slide. It was 28 mm long and composed of 7 parallel grooves that terminated in plenums on both ends. The grooves and plenums were machined via an ultrasonic milling process. The cross section of each channel was 1 mm wide by 0.6 mm deep, and the spacing between the channels was 1 mm.

Several shapes and locations of electrodes were tested. The configuration producing the best results is shown in Fig. 1. The electrode pair sandwiches the groove in the evaporator section as shown in Figs. 1c and 1d. From Fig. 1c, it can be seen that the high-voltage electrodes were directly attached to the 1-mm-thick cover slide adhered to the open side of the grooves; hence, the electrode was in intimate contact with the liquid. The ground electrodes were attached to the exterior surface of the grooved slide. Therefore, the spacing between two electrodes of different levels is 1 mm. The electrodes were fashioned out of aluminum foil. The application of the high-voltage across the electrodes was achieved using a high-voltage dc power supply. The voltage was monitored using a high-voltage meter. The uncertainty of the measurement is ± 10 V. The current was also measured using a microamperes meter. The current at 8 kV is 10 ± 1 μA. Therefore, the power dissipation was estimated to be 0.08 W, which is less than 3% of the heat input to the micro heat pipe.

Heat was input to the heat pipe array via an electric resistance heater element located just at the end of channels on the evaporator side as shown in Fig. 1. Heat was rejected by pumping 5 ± 0.5°C deionized water through a cooling jacket attached to the micro heat pipe array on the condenser side. The entire facility was insulated with 5 cm of ceramic fiber insulation to ensure that all heat was

rejected through the cooling jacket. Heat losses were estimated to be less than 5% of the total heat input.

Five calibrated thermocouples were attached to the micro heat pipe array with thermally conducting epoxy. These thermocouples were distributed along the central channel with spacing of 5.5 mm. They were used to monitor micro heat pipe temperature in the tests. Every test continued until steady state was reached, usually taking 24–30 min. The uncertainty associated with the temperature measurement was less than ±0.2°C.

The working fluid used in the experiments was pentane, a dielectric fluid with high vapor pressure. Its permittivity $\varepsilon_l = 1.8371$, and its electrical conductivity $\sigma_e \leq 2 \times 10^{-10}$ ohm$^{-1} \cdot$ cm^{-1} at 20°C (Ref. 20). The permittivity of the glass $\varepsilon_s = 7.0$ (Ref. 21). The micro heat pipe array was posed at a 9-deg tilt angle, with the evaporator elevated above the condenser. This initial inclination was only necessary at startup. The applied electric field intensities were 4, 6, 8, and 9.5 kV/mm. At 10 kV/mm, breakdown occurs. Tests without an electric field were also conducted to serve as a baseline for tests conducted with electric field applied. The heat inputs considered were 1 W and 1.5, 2, 2.5, and 3 ± 0.1 W, respectively, for each of the four different electric field intensities. The micro heat pipes were filled with pentane with 30, 40, 52, and 60 ± 5% liquid volume fractions at ambient conditions.

The experimental test procedure was as follows. First the deionized water was pumped through the cooling jacket. The electric field and heat input were established simultaneously. The wall temperatures were monitored until steady state was reached, at which time the heat input and electric field were discontinued. Some experiments were conducted with the micro heat pipe visible. The transparent structure permitted visualization of the internal fluid orientation. A high-resolution camera with 8-mm tape was used to provide a video record of the operation to better understand its functioning.

Results and Discussion

The experiments conducted were mainly focused on investigating the influence of the applied electrostatic field on the maximum heat transport capacity. The experimental maximum heat transport capacity was determined in the following way. For an applied electric field strength and heat input, the experiment continued until the wall temperature reached a steady-state value. When the maximum heat transport capacity was reached, dry out conditions in the evaporator caused the evaporator temperature to rise rapidly.

The transient temperatures were recorded using an IoTech temperature measurement system, TempScan/1000. One of the typical datum is plotted in Fig. 3. At 2.5-W heat input, the lowest maximum temperatures at steady state were obtained under 8- and 6-kV electric field intensities. In the no electric field case, no steady state existed. The evaporator dried out very fast. This indicates that the electric field dramatically promotes the heat transport capability of micro

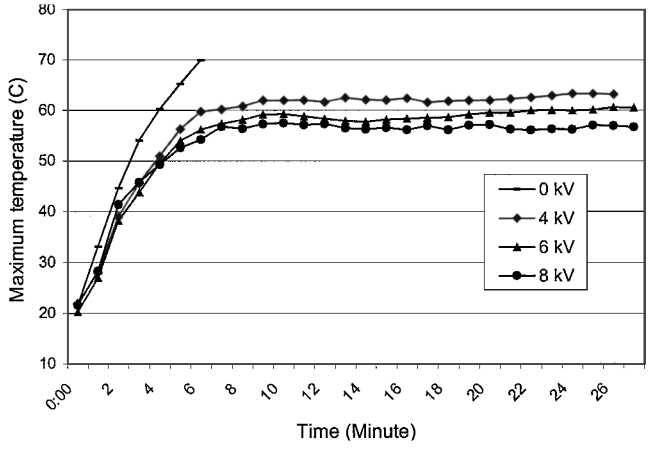

Fig. 3 Temperatures vs time at 2.5 W under various operating voltages.

Table 1 Ratio of EHD driving potential and capillary pressure potential to total driving potential

Electric field intensity, kV/mm	$\Delta P_{electr}/\Delta P_{total}$, %	$\Delta P_{cap}/\Delta P_{total}$, %
0	0	100
4	63.3	36.7
6	79.5	20.5
8	87.3	12.7
9.5	90.7	9.3

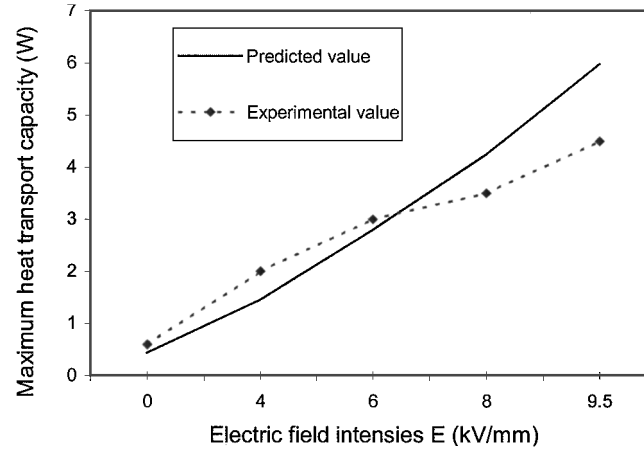

Fig. 4 Predicted and experimental maximum heat transport capacity vs electric field intensity.

heat pipes because of the application of electric field collecting more working liquid at the evaporator. It was observed that thick liquid films were formed in the evaporator region due to the collection effect of the electric field.

Taking the contact angle as 0, C_1, and C_2 were calculated equal to 1.155 and 0.42, respectively, using the formulas derived by Ma and Peterson.[6] Constant C^* was found to be 1.65 based on Eq. (8). A value of 16 was taken for $f_v \cdot Re_{h,v}$ and 15 for $f_l \cdot Re_{h,l}$ according to the geometry of the duct.[22] When these values were substituted into Eq. (10), the maximum heat transport capabilities were evaluated. The model permitted prediction of the maximum heat transport capacity for various electric field intensities. Both the experimental results and the model predictions for the maximum heat transport capacity as a function of the electric field intensity are shown in Fig. 4. Good agreement between predicted values and experimental data is achieved. In Fig. 4, both experimental data and model predictions show that increasing electric field intensity causes an increase in the maximum heat transport capacity. Most significantly, the experimental results suggest about a six-time improvement in the maximum heat transport capacity at the greatest electric field considered (9.5 kV/mm), above which corona discharge was evident.

In evaluating the heat transport capacity using Eq. (10), it is found that, with an increase in the electric field intensity, the proportion of the EHD potential to the total driving potential increases. This increase in heat transport capacity with electric field is better visualized by looking at the relative importance of the EHD driving force to capillary force as a function of the electric field, as shown in Table 1. Here ΔP_{total} represents the total driving pressure. It can be seen from Table 1 that the EHD potential becomes the dominant driving force at high electric fields, constituting 87.3% of the driving potential at an electric field of 8 kV/mm. The experimental data demonstrate the same trend, as shown in Fig. 5. At the same heat input, for example, 2.5 W, as electric field increases, the heat transport capacity increases, leading to the maximum temperature in the micro heat pipe going down, from 72°C at 4 kV to 57°C at 8 kV.

With the verification of the applicability of the model in predicting the performance of one EHD micro heat pipe, the developed model can also be used to analyze geometrical and parametric variations of the EHD micro heat pipes. When the spacing between the grooves

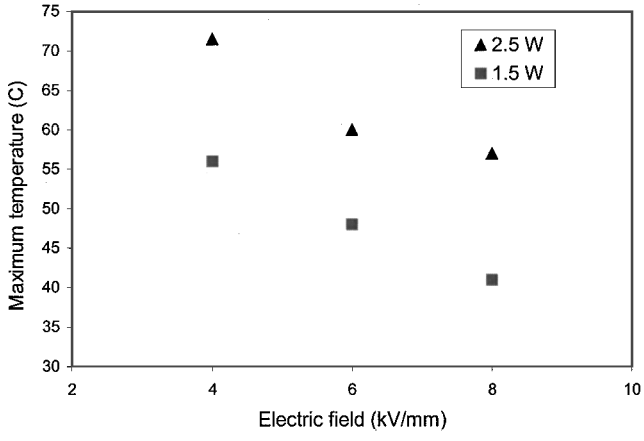

Fig. 5 Experimental results of electric field influence on heat transport capacity of micro heat pipes.

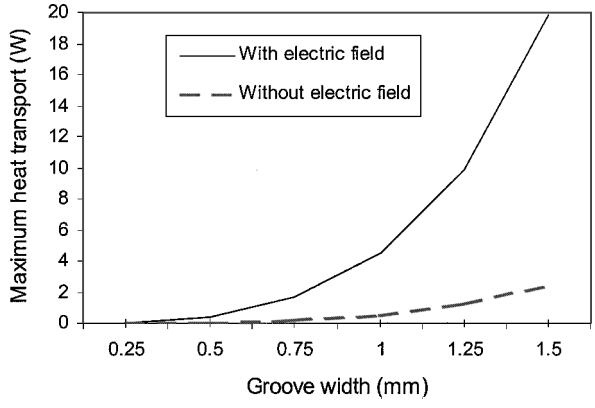

Fig. 6 Theoretical maximum heat transport capacity vs groove width with and without an applied electric field of 8 kV/mm.

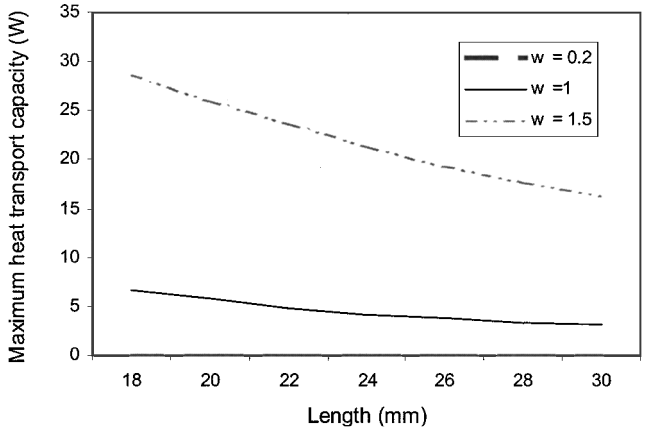

Fig. 7 Theoretical maximum heat transport capacity vs length of the pipe with various groove widths at 8 kV/mm.

d is set to be two times the width of a groove, that is, $d = 2w$ and L, the length of a channel, the relationship between the maximum heat transport capacity and the groove width is revealed to be $q \propto w^4$, and it is plotted in Fig. 6. In this evaluation, the electric field is fixed at 8 kV/mm and the micro heat pipe length is 22 mm. Figure 6 shows that the maximum heat transfer capacity of EHD micro heat pipes is achieved when the groove width is maximized. Note that this would only be true for Bond numbers less than unity. The relationship between q and w for zero electric field is approximately $q \propto w^2$. Interestingly, EHD micro heat pipes receive more benefit from larger pore sizes than conventional micro heat pipes.

The relationship between the maximum heat transfer capacity and the length L is also obtained at 8 kV/mm and is plotted in Fig. 7. Figure 7 shows the effect of micro heat pipe length for various groove

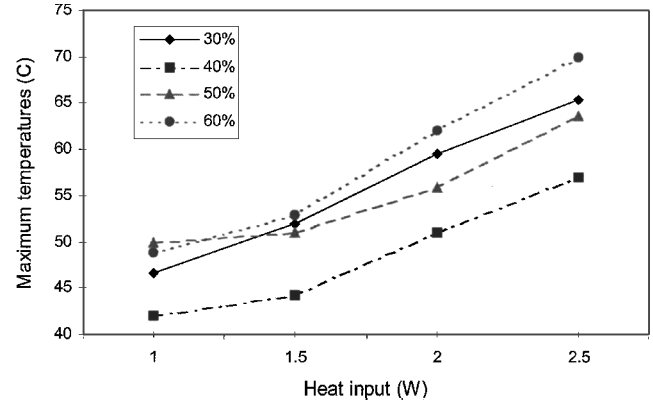

Fig. 8 Maximum heat pipe temperatures vs heat input for various liquid volume fractions under 8 kV/mm.

widths on maximum heat transport capacity. When combined, these results suggest that a wider and shorter micro heat pipe is optimum. Similar conclusions were drawn by Longtin et al.[3] for conventional micro heat pipes.

The amount of filled liquid is also an important factor for EHD micro heat pipe operation. Four different fill levels were tested in present experiments, and the results are shown in Fig. 8. The best performance of EHD micro heat pipes is achieved in the 40% case because of the lowest maximum temperatures at steady state. It was observed that when redundant liquid was filled, for example, 60%, flooding occurred in the condenser region, which obstructed vapor to reach the condenser and, therefore, degraded the performance of the EHD micro heat pipes. When the fill amount was small, for example, 30%, no sufficient liquid could be supplied for evaporation; therefore, EHD micro heat pipes can not operate properly. The preceding discussion implies that the fill amount of liquid should be sufficient for the forming of a capillary artery and while no flooding occurs in the condenser. Therefore, the fill amount of liquid in EHD micro heat pipes is a complex issue.

The electric charge relaxation time τ_e is estimated to evaluate the impact of the liquid motion on the electric field. For present experimental model, $\tau_e = \varepsilon_l/\sigma_e \approx 1.62 \times 10^{-3}$ s. The velocity of fluid traveling was determined by $U = q''/(\rho_l \lambda)$. Thus, electric Reynolds number $Re_{\mathrm{EHD}} = \varepsilon_l U/(\sigma_e L_{\mathrm{eff}}) = 3.24 \times 10^{-3}$. $Re_{\mathrm{EHD}} \ll 1$, and so the field and charge distribution are not appreciably influenced by the liquid motion.

Closer inspection of the model predictions finds that the vapor pressure drop only accounts for 0.8% and the pressure drop in the liquid slug accounts for 0.2% of the total pressure drop, respectively, in the micro heat pipe. This implies that all of the pressure drops are confined to the liquid film surrounding the trapped vapor bubble in the liquid supply channels (Fig. 2). This result indicates that if the trapped vapor bubble can be eliminated, much greater heat transport capacity should be obtained. This ideal condition may be achieved if the electrodes fully cover the liquid supply channels, as shown in Fig. 9. The application of electric field makes the channels covered by electrodes fully filled with working liquid. In this scenario, the pressure drops are shown in Fig. 9b, and Eq. (1) becomes

$$\Delta P_{\mathrm{EHD}} + \Delta P_c \geq \Delta P_v + \Delta P_{\mathrm{slug}} \tag{13}$$

The heat transport capacity is then expressed as

$$q = (1/M')\left[\varepsilon_0(\varepsilon_l - \varepsilon_v)(E^2/2) + \sigma(1/r_{c,e} - 1/r_{c,c})\right] \tag{14}$$

where M' is expressed as

$$M' = \frac{12\mu_l L_{\mathrm{slug}}}{wa^3\rho_l\lambda} + \frac{f_v Re_{h,v}\mu_v L_{\mathrm{eff}}}{2r_{h,v}^2 A_v \rho_v \lambda} \tag{15}$$

A comparison of the model predictions on heat transport capacity for a fully and partially liquid filled evaporator channel as a function of electric field is shown in Fig. 10. Here, fully liquid filled means

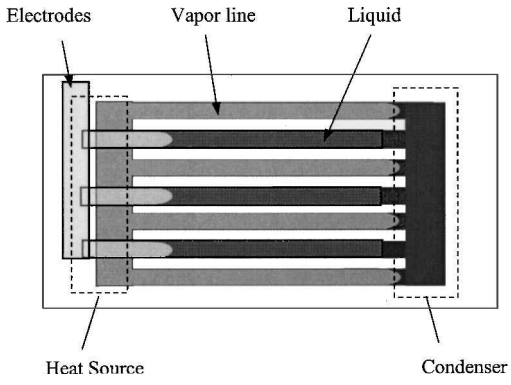

Fig. 9a Liquid fully filled schematic (ideal model).

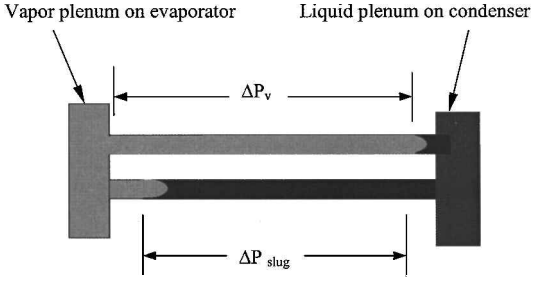

Fig. 9b Pressure drops in liquid fully filled case.

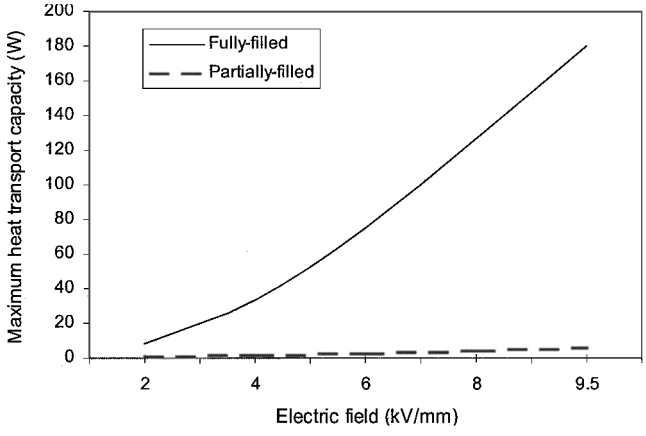

Fig. 10 Predictions of maximum heat transfer capacity vs electric field for fully liquid filled and partially liquid filled micro heat pipes.

the whole channel beneath the electrode was fully filled with liquid when electric field applied as shown in Fig. 9; partially liquid filled means the channel beneath the electrode was partially (50%) filled with liquid as shown in Fig. 1b. Clearly, elimination of the entrapped vapor bubble can substantially increase the heat transport capacity of the micro heat pipe. In this case, up to a 180-fold increase in the heat transport capacity is predicted.

Experimentally, electrodes were fashioned to cover the whole liquid supply channels. The micro heat pipe was charged with a 50% liquid volume fraction at ambient conditions as shown in Fig. 9a. The maximum heat transport capacity measured experimentally was observed to be substantially less than the very optimistic predictions, as shown in Fig. 11. It is observed in experiments that the ideal loop heat transfer mode, as shown in Fig. 9b, was not implemented in the whole micro heat pipe array. Only one or two of the four vapor return channels served for their function during experiments. Other vapor return channels were filled with liquid, which hindered the vapor return and, therefore, degraded the function of the micro loop system. The reason for the phenomenon may be that the actual electric field was not uniform and its distribution was fairly complicated.

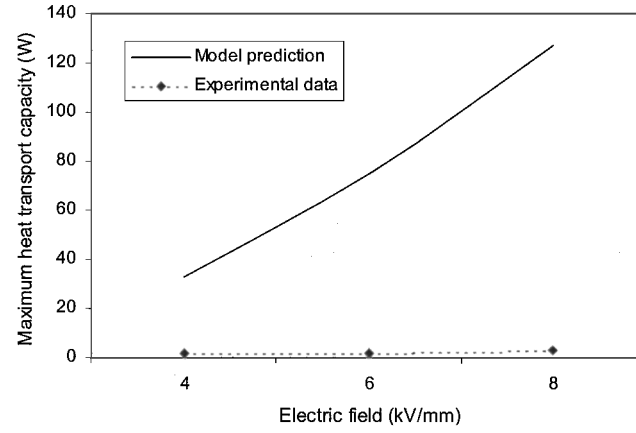

Fig. 11 Model predictions and experimental data of maximum heat transport capacity for ideal model (fully liquid filled) micro heat pipes.

Although the electrodes did not cover the vapor return channels, the electric field was still so strong that liquid was collected in those channels and obstructed the vapor back to the condenser. This phenomenon, however, is not indicative of the inherent failure of this concept. Rather, it suggests a remedy that should be addressed in future design. The high-voltage and ground-level electrodes in the evaporating channels should be in intimate contact with the liquid. As well, the vapor return line should be completely shielded from the electric field. Such a design is expected to be the optimum one.

Conclusions

A mathematical model to predict the maximum heat transport capacity of electrohydrodynamic micro heat pipes vs electric field intensity is presented. Good agreement is achieved in comparing the predicted value with the experimental data. Equation (10) indicates that increasing applied electric field can increase the maximum heat transport capacity of EHD micro heat pipes because, at high level electric field, the EHD driving force became dominant. The optimum geometry of the EHD micro heat pipe can also be predicted using Eq. (10). The prediction indicates that the optimum EHD micro heat pipe is short and wide with the requirement that the Bond number be less than one. An ideal configuration of the EHD micro heat pipe is predicted by Eq. (10). The ideal EHD micro heat pipe model should have specially shielded vapor return channels for the vapor to reach condenser rapidly. Equation (10) can be used to predict the performance of EHD micro heat pipes and to aid the future design of the pipes.

Acknowledgment

The authors are indebted to Thomas B. Jones for his invaluable advice on this paper.

References

[1]Cotter, T. P., "Principles and Prospects for Micro Heat Pipes," *Proceedings of the 5th International Heat Pipe Conference*, Japan Association for Heat Pipes, Tsukuba, Japan, 1984, pp. 328–335.

[2]Babin, B. R., Peterson, G. P., and Wu, D., "Steady-State Modeling and Testing of a Micro Heat Pipe," *Journal of Heat Transfer*, Vol. 112, Aug. 1990, pp. 595–601.

[3]Longtin, J. P., Badran, B., and Gerner, F. M., "A One-Dimensional Model of a Micro Heat Pipe During Steady-State Operation," *Journal of Heat Transfer*, Vol. 116, Aug. 1994, pp. 709–715.

[4]Khrustalev, D., and Faghri, A., "Heat Transfer During Evaporation on Capillary-Grooved Structures of Heat Pipes," *Journal of Heat Transfer*, Vol. 117, Aug. 1995, pp. 740–747.

[5]Ma, H. B., and Peterson, G. P., "Experimental Investigation of the Maximum Heat Transport in Triangular Grooves," *Journal of Heat Transfer*, Vol. 118, Aug. 1996, pp. 740–746.

[6]Ma, H. B., and Peterson, G. P., "The Minimum Meniscus Radius and Capillary Heat Transport Limit in Micro Heat Pipes," *Journal of Heat Transfer*, Vol. 120, Feb. 1998, pp. 227–233.

[7]Peterson, G. P., and Ma, H. B., "Temperature Response of Heat Transport in a Micro Heat Pipe," *Journal of Heat Transfer*, Vol. 121, May 1999, pp. 438–445.

[8]Cao, Y., Faghri, A., and Mahefkey, E. T., "Micro/Miniature Heat Pipes and Operating Limitations," ASME Annual Meeting, HTD-Vol. 236, American Society of Mechanical Engineers, Fairfield, NJ, 1993, pp. 55–62.

[9]Peterson, G. P., *An Introduction to Heat Pipes*, Wiley, New York, 1994, Chaps. 3, 6.

[10]Faghri, A., *Heat Pipe Science and Technology*, Taylor and Francis, Washington, DC, 1995, Chap. 10.

[11]Jones, T. B., "Electrohydrodynamic Heat Pipes," *International Journal of Heat and Mass Transfer*, Vol. 16, No. 5, 1973, pp. 1045–1048.

[12]Jones, T. B., and Perry, M. P., "Electrohydrodynamic Heat Pipe Experiments," *Journal of Applied Physics*, Vol. 45, No. 5, 1974, pp. 2129–2132.

[13]Jones, T. B., "An Electrohydrodynamic Heat Pipe," *Mechanical Engineering*, Vol. 96, Jan. 1974, pp. 27–32.

[14]Loehrke, R. I., and Debs, R. J., "Measurements of the Performance of an Electrohydrodynamic Heat Pipe," AIAA Paper 75-659, May 1975.

[15]Bryan, J. E., and Seyed-Yagoobi, J., "Heat Transport Enhancement of Monogroove Heat Pipe with Electrohydrodynamic Pumping," *Journal of Thermophysics and Heat Transfer*, Vol. 11, No. 3, 1997, pp. 454–460.

[16]Hallinan, K. P., Bhagat, W. W., Kashaboina, B., and Kashani, R., "Electrohydrodynamic Augmentation of Heat Transport in Micro Heat Pipe Arrays," American Society of Mechanical Engineers, HTD Vol. 361-3, Anaheim, CA, 1998, pp. 165–171.

[17]Melcher, J. R., "Electric Field and Moving Media," *IEEE Transactions on Education*, Vol. E-17, No. 2, 1974, pp. 100–110.

[18]Crowley, J. M., *Fundamentals of Applied Electrostatics*, Wiley, New York, 1986, pp. 19, 20, 161–167.

[19]DI Marco, P., and Grassi, W., "Saturated Pool Boiling Enhancement by Means of an Electric Field," *Enhanced Heat Transfer*, Vol. 1, No. 1, 1993, pp. 99–114.

[20]Dean, J. A., *Lange's Handbook of Chemistry*, McGraw–Hill, New York, 1992, pp. 5.118, 8.163.

[21]Shand, E. B., *Glass Engineering Handbook*, McGraw–Hill, New York, 1958, pp. 17, 18.

[22]Bejan, A., *Convection Heat Transfer*, Wiley, New York, 1995, pp. 100–105.